JOURNAL OF THERMOPHYSICS AND HEAT TRANSFER
Vol. 21, No. 3, July–September 2007

Thermal Modeling and Testing of a Nanosatellite's Avionics Board

Stephen W. Miller*
NASA Johnson Space Center, Houston, Texas 77058
and
Ed Marotta†
Texas A&M University, College Station, Texas 77843

DOI: 10.2514/1.26659

A lumped-capacitance thermal model of an avionics board within the Miniature Autonomous Extravehicular Robotic Camera was developed to predict component temperatures. Subsequently, a thermal vacuum test was conducted to determine the board's measured thermophysical properties and validate temperature predictions. A functional prototype of the board was instrumented with 24 type-T thermocouples and placed in a thermal vacuum chamber. The board was then subjected to two power conditions while the temperature response was recorded. Analysis of the data shows that the measured values of the in-plane thermal conductivity are dominated by the dielectric material. Pretest analysis underpredicted the through-plane thermal conductivity by 63% and the in-plane thermal conductivity was overpredicted by approximately 740%. Additionally, the bulk emissivity of the board was determined using an average temperature of the thermocouples on the back side of the board. The emissivity calculated from measured temperature data, 0.95, was approximately 19% higher than the assumed emissivity used in pretest models, 0.80. Incorporation of the thermophysical properties based on measured data allows the updated model to predict temperatures of the LED board within an uncertainty of ±10°C and to capture the transient response of the board with considerable accuracy.

Nomenclature

A_{cs}	=	cross-sectional area, m^2
A_i	=	area, m^2
$A_{surface}$	=	surface area, m^2
c_p	=	specific heat, $J/(kg \cdot K)$
I	=	current, A or mA
k_i	=	thermal conductivity, $W/(m \cdot K)$
L_i	=	length, m
m	=	mass, kg
N_{LED}	=	number of LEDs
P	=	power, W
$\dot{Q}$	=	energy transfer rate, W
$\dot{Q}''$	=	heat flux, W/m^2
R_i	=	thermal resistance, K/W
r_i	=	radius, m
s_i	=	length, m
T_C	=	thermocouple temperature, K
T_i	=	temperature, K or C
T_{sink}	=	sink temperature, K
t_i	=	thickness, m
V	=	voltage, V
ε	=	emissivity
σ	=	Stefan–Boltzmann constant, 5.67×10^{-8} $[W/(m^2 \cdot K^4)]$

I. Introduction

THE Miniature Autonomous Extravehicular Robotic Camera (Mini-AERCam) is a nanoclass free-flying satellite intended to provide unique camera views for various space-related applications. Examples of its potential functionality include inspecting space shuttle thermal protection system surfaces, providing reconnaissance photographs before and after an extravehicular activity (space walk or robotic task), and imaging rendezvous/docking maneuvers from unique vantage points [1–4]. A technology demonstration unit developed at the Johnson Space Center is approximately 216 mm in diameter and weighs approximately 57.9 N. It contains a propulsion system, battery power system, and a full suite of avionics, including communications, video processing, and guidance, navigation, and control. The Mini-AERCam also contains two separate high resolution cameras, one used for navigation and the other for inspection/imaging. Figure 1 shows an exploded view of the Mini-AERCam satellite.

As part of the inspection unit, the Mini-AERCam contains a light emitting diode (LED)[‡] board that illuminates surfaces under inspection. The LED board is located external to the main shell structure and allows the inspection camera lens to protrude through its center. The LEDs are pulsed on when additional illumination is desired for imaging, and when the LED array is employed as part of a sensor for target-based docking navigation.

To accurately model the thermal characteristics of the Mini-AERCam as a whole and the LED board in particular, it is essential to have reliable values for thermophysical properties such as thermal conductivity and emissivity. Although these properties can be calculated or estimated from past experience, test data provide the most reliable means of obtaining accurate values. Therefore, a thermal vacuum test of the LED board was conducted to determine its thermophysical properties. The values obtained can be extended to other avionics boards in the Mini-AERCam until a complete thermal vacuum test of the system can be performed.

Presented as Paper 3279 at the 9th AIAA/ASME Joint Thermophysics and Heat Transfer Conference, San Francisco, CA, 5–8 June 2006; received 19 July 2006; revision received 10 October 2006; accepted for publication 28 November 2006.

*Aerospace Engineer, Heat Transfer, Thermal Design Branch, ES3; stephen.w.miller@nasa.gov.

†Associate Professor, Mechanical Engineering, 315 Engineering/Physics Building; emarotta@tamu.edu. Associate Fellow AIAA.

‡"Specification for Nichia White LED Model: NSPW312BS," Nichia Corporation (online technical database) http://www.nichia.co.jp/product/led-lamp-phi3.html [retrieved 9 June 2005].

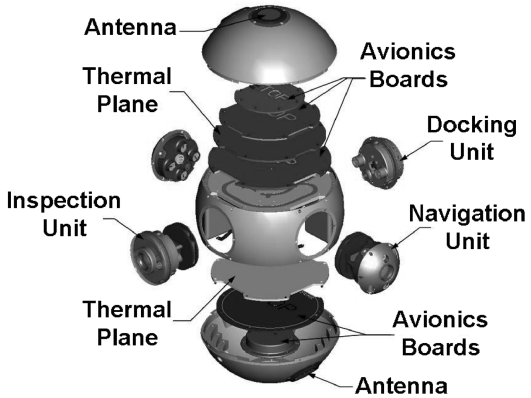

Fig. 1 Exploded view of the Mini-AERCam.

The specific objectives of the analytical and experimental study were to present the following: 1) both estimated and measured thermophysical properties for the LED board, 2) a numerical investigation for the transient and steady-state temperatures within the LED board at various power levels, 3) data anomalies observed, and 4) updated model predictions based on measured thermophysical properties. The manuscript is organized as follows. The mathematical formulations employed for the initially computed values for thermal conductivity and surface emissivity are described in Sec. II. The experimental program is described in Sec. III. A presentation of the test data and conclusions and discussions of the various points of interest gleaned from the data are given in Sec. IV. Thermal models were updated and an attempt to replicate the test data with model runs is given in Sec. V. Finally, uncertainty analysis and conclusions are given in Secs. VI and VII, respectively.

II. Mathematical Formulations

Before testing the LED board, the thermophysical properties were calculated based on dimensioned drawings and thermal properties obtained from various handbooks. Of specific interest were the thermal conductivity (in-plane and through-plane values) and emissivity. These properties affect the thermal performance of any space-related vehicle.

To calculate the thermal conductivity, drawings of the LED board layout were obtained, including the individual layer thicknesses and materials (see Fig. 2) [5]. A thermal resistance network was developed for both the in-plane and through-plane paths, which allowed for the in-plane and through-plane thermal conductivities to be calculated. Several simplifying assumptions for these calculations were made:

1) The board is a solid cylinder. Cutouts for the camera and thrusters are ignored.

2) The copper layers are solid planes. No material is etched away.

3) The effect of small donut-shaped conductors called vias and other small components is ignored.

4) The material properties of each layer are isotropic.

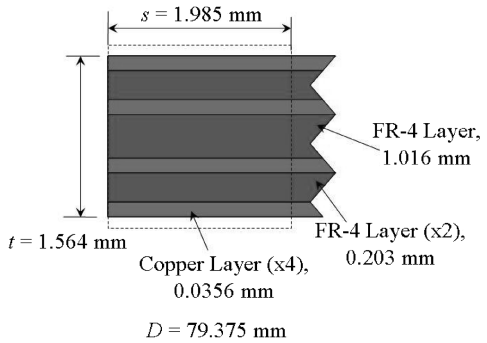

Fig. 2 LED board dimensions and materials used in calculating thermophysical properties.

Table 1 Material properties for copper and FR-4

Material	Property	Value
Copper	Thermal conductivity	391.15 W/(m · K)
	Density	8940 kg/m^3
FR-4	Thermal conductivity	0.2942 W/(m · K)
	Density	1794 kg/m^3

5) All power input is dissipated as heat into the board.

Additionally, the material properties used for copper and FR-4 are listed in Table 1.

For calculation of the in-plane thermal conductivity, the resistances are in parallel, as shown in Fig. 3. Therefore, the reciprocal of the total resistance is the sum of the reciprocal of the individual resistances. To calculate the individual resistances, the board is divided into a rectangular grid with an edge length s of 1.985 mm. The grid edge length is used to calculate both the cross-sectional area, A and A_i, as well as the length, L_i and L_{total}. Using this approach the calculated value for the in-plane thermal conductivity was computed as 36.2 W/(m · K).

$$R_i = \frac{L_i}{k_i A_i} \tag{1}$$

$$\frac{1}{R_{\text{in-plane}}} = \sum \frac{1}{R_i} = \frac{k_{\text{in-plane}} A_{\text{total}}}{L_{\text{total}}} \tag{2}$$

$$L_i = L_{\text{total}} = s_{\text{grid}} \tag{3}$$

$$A_i = t_{\text{layer}} s_{\text{grid}}, \qquad A_{\text{total}} = t_{\text{board}} s_{\text{grid}} \tag{4}$$

For calculation of the through-plane thermal conductivity, the resistances are in series as shown in Fig. 4. Therefore, the total resistance is the sum of the individual resistances. To calculate the individual resistances, the cross-sectional area of the board was set equal to the surface area of one face, whereas L_i is simply the thickness of the particular layer being considered. Using this approach the calculated value for the through-plane thermal conductivity was computed as 0.32 W/(m · K).

$$R_i = \frac{L_i}{k_i A_i} \tag{5}$$

$$\frac{1}{R_{\text{through-plane}}} = \sum R_i = \frac{L_{\text{total}}}{k_{\text{through-plane}} A} \tag{6}$$

$$L_{\text{total}} = t_{\text{board}} \tag{7}$$

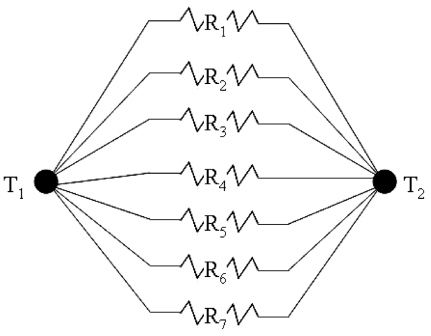

Fig. 3 In-plane thermal resistance network.

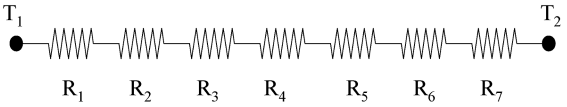

Fig. 4 Through-plane thermal resistance network.

$$A = A_i = \frac{\pi}{4} D^2, \qquad L_i = t_{\text{layer}} \tag{8}$$

The emissivity of the LED board was initially assumed to be 0.8. A summary of the calculated thermophysical properties is presented in Table 2.

A. LED Board Thermal Model

A lumped-capacitance thermal math model of the LED board was built using a graphical interface to a numerical solution program (see Fig. 5). The graphical interface allows the geometry of the part to be built and nodalized by the user. Additionally, material properties can be assigned to individual components and conduction paths established between nodes. The graphical interface also features a radiation analysis tool, which uses a Monte Carlo ray tracing algorithm to determine radiation exchange between surfaces and their surroundings. All of this nodalized information was combined into a lumped parameter thermal resistance network analyzer to solve for both steady-state and transient temperature profiles.

The geometric model of the LED board consists of a disk with an outer diameter of 79.375 mm, an inner diameter of 27.94 mm, and a thickness of 1.566 mm. The thickness was used only to calculate the capacitance of the board. Because the disk is a 2-D object only, no through-plane effects are modeled. The board was assigned material properties for conductivity and emissivity as described previously. The board was divided into 12 angular and 6 radial regions, each with a body-centered node. Therefore the LED board thermal model consists of 72 nodes.

All 160 LEDs are individually modeled as semispherical surfaces. These surfaces have a diameter of 3.8 mm and are given the thermophysical properties associated with fused silica (see Table 3). Each LED was represented by a single node.

Because the heat load is generated by the LEDs it is important to model the resistance between the LEDs and the board itself. Therefore, the leads of the LEDs are considered to be the primary heat transfer source between the LEDs and the board. Each LED consists of 2 copper leads, each with a diameter of 0.5 and 4 mm long. The resistance from each lead can be calculated by

$$R_{\text{lead}} = L/(kA_{\text{cs}}) \tag{9}$$

Inserting the appropriate values yielded a thermal resistance of 52.2 K/W per lead. Because the leads provide a parallel path, the total resistance was

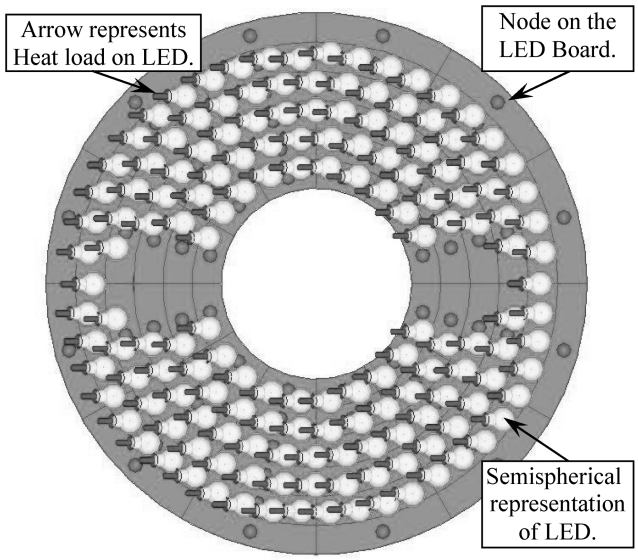

Fig. 5 Geometric model of the LED board.

$$R_{\text{total}} = 1/(1/R_{\text{lead},1} + 1/R_{\text{lead},2}) \tag{10}$$

which yields a total resistance $R_{\text{tot}} = 26.1$ K/W. This value was applied as the resistance between each LED node and the closest node on the LED board.

The graphical interface also allows the user to enter a heat load. To be consistent with the planned test cases and capabilities of the LED board, two separate heat loads were applied. The first heat load placed a total of 0.625 W on the inner ring of LEDs (20 LEDs). The other heat load placed 4.375 W on the remaining 140 LEDs. The heat loads were managed such that only the inner ring heat load was active, both heat loads were active, or no heat loads were active.

B. Model Predictions

Several thermal analysis cases were run that mimicked the planned test cases. All of these cases assumed a constant radiation environment of −20°C in a vacuum. The analysis cases are presented in Table 4, followed by a brief description of each case. The −20°C environment was chosen to allow the LED board to operate within its temperature limits of −30 to 85°C.

The initial cold soak provides insight into the thermal capacitance of the board. The transient cool down from ambient temperatures to −20°C depends largely on the specific heat and emissivity assigned to the materials.

Powering only the inner ring of LEDs with 0.625 W produces the largest temperature gradient between the inner and outer edges of the LED board. This configuration allows the in-plane thermal conductivity to be measured.

Table 2 Calculated thermophysical properties of the LED board

Property	Value
In-plane thermal conductivity	36.2 W/(m · K)
Through-plane thermal conductivity	0.32 W/(m · K)
Emissivity	0.8

Table 3 Thermophysical properties of fused silica

Property	Value
Thermal conductivity	1.5 W/(m · K)
Emissivity	0.9

Table 4 LED board thermal vacuum test cases

Case	Initial temperature, °C	Final temperature, °C	Power input, W	Time to reach steady state, h
Initial cold soak	25	−20	0	1.0
Inner ring of LEDs powered	−20	1	0.625	1.0
All LEDs powered	1	84	5.0	0.8
All LEDs off	84	−20	0	1.2

Turning on all LEDs places full power into the board and allows for determination of the through-plane thermal conductivity, as well as the emissivity. The model predicted temperatures quickly reached 84°C, which is within 1°C of the upper temperature limit of the LEDs. Therefore, this was determined to be a critical phase of testing when temperatures would be monitored closely. To protect the hardware, power to the LED board will be removed if the temperatures approached the defined limit.

The final unpowered test segment provides an additional opportunity to determine the thermal capacitance of the LED board. Because the board starts from a higher temperature, there exists a longer transient period that allows better characterization of the emissivity.

III. Experimental Study

An objective of the experimental study was to obtain temperature and power data needed to determine the thermophysical properties and characteristics of the Mini-AERCam LED board [6]. The data collected were compared against the results from thermal model predictions. The thermal model was then updated in an attempt to more closely match the test results.

A. Test Article Description

The test article was a prototype of the Mini-AERCam LED board. A large center hole allows a camera lens to view the illuminated surface and two smaller holes provide openings for thrusters that control the vehicle's orientation and movement. The board contains 160 LEDs.

B. Instrumentation

Before the test, 24 type-T thermocouples (TC) were installed on the test article. Type-T thermocouples were chosen because they are compatible with the facility infrastructure, functional within the predicted temperature ranges for the test, and accurate to ±0.5°C. The TCs were installed to provide a uniform temperature profile for both faces of the board as seen in Fig. 6. The radial pattern of the TCs allows for the determination of the in-plane thermal conductivity. Additionally, installing TCs on opposite sides of the board allows for the through-plane thermal conductivity to be measured. The TCs were installed using a fast curing epoxy, which was allowed to set overnight before the test article was handled.

C. Power to Test Article

The LEDs receive power via 6 small input wires at the top of the board. The power architecture allows for 4 separate power configurations:

1) Unpowered;
2) Inner ring of LEDs on;
3) All LEDs except inner ring on;
4) All LEDs on.

During the test, only configurations 1, 2, and 4 were used.

During the test, both V and I into the board were monitored. To achieve the desired power levels on the board, the voltage at the power supply unit was varied until the power into the board was at the appropriate value.

D. Chamber Facility and Support Structure

The test was conducted at the Johnson Space Center Building 33, Chamber G. This is a small thermal vacuum chamber which provided an internal shroud that can be controlled to a desired temperature by using liquid or gaseous nitrogen. The chamber contains a central plate for mounting the hardware and a window through which the test article can be observed during the test.

The test article was mounted to an aluminum I-beam by two small screws. To minimize conduction losses to the support structure, Teflon standoffs separated the board from the I-beam and the screw/nut interface from the I-beam. Figure 7 shows the test article mounted to the I-beam and installed in the test chamber. Additionally, the aluminum I-beam was set on Teflon blocks to minimize its interface with the chamber structure.

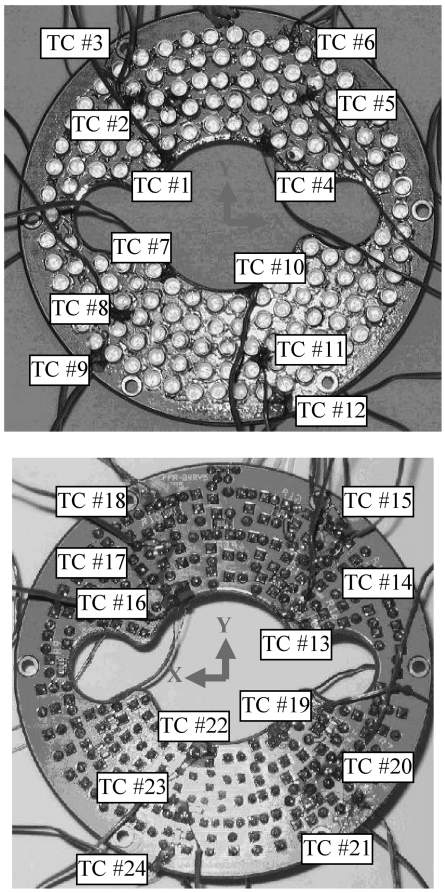

Fig. 6 TC installation pattern on LED board front and back surfaces.

E. Shroud Temperature, Power Profile, and Data Acquisition

The planned shroud temperature profile called for the shroud to remain at −20°C for the duration of the test. This temperature permits the LED board to remain within upper and lower temperature limits for all power configurations per pretest thermal model predictions.

The planned power profile required three power levels: no LEDs powered (0 W), the inner ring of LEDs powered (0.625 W), and all LEDs powered (5.0 W). Two complete cycles were planned to gather data on repeatability and to capture valid data at all power levels. During the test, data were recorded once every 30 s. This includes all 24 thermocouples, inner LED ring voltage/current, outer LED ring

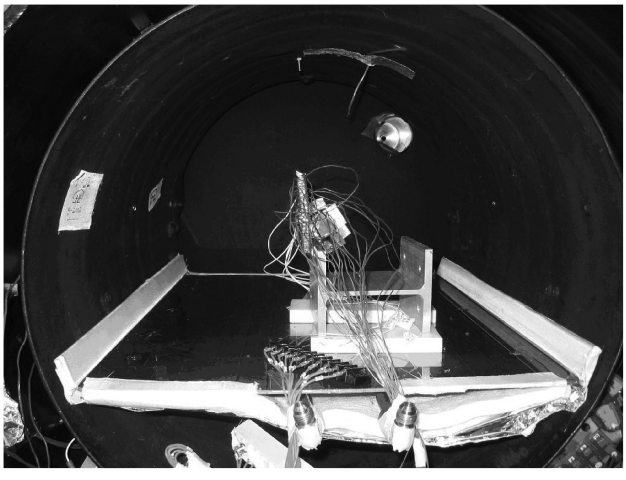

Fig. 7 Test article installed inside test chamber shroud.

voltage/current, chamber pressure, and shroud temperatures. To minimize the effects of convection, the test was conducted at a pressure of less than 1×10^{-4} torr.

IV. Results and Discussion

The measured data provided an opportunity to determine the actual thermophysical properties of the LED board. In turn, these measured values were used to verify and update the thermal model predictions of the LED board. The following sections present the test data and discuss various points of interest gleaned from the data.

A. Chamber Shroud Temperature Profile

The shroud temperature was maintained at the desired $-20°C \pm 2°C$ for the duration of the test periods. There were no problems with the chamber shroud temperature control during the test.

B. Measured Power, Voltage, and Current Profile

The measured power profile as a function of time is presented in Fig. 8. Note that during the first "all LEDs on" period, there was a brief period of time (less than 3 min of the 60 min heating cycle) when the voltage exceeded 5.0 W. This was caused by the current through the LEDs increasing as their temperatures increased. Figure 9 plots both the current and voltage as a function of time and shows the "sawtooth" pattern of the current. To compensate for this change, the voltage was manually decreased to maintain the desired power level. The excess energy input caused by the rising current draw was approximately 1.3% of the nominal energy input as estimated from voltages in Fig. 9.

C. Measured Temperatures

In presenting the temperature data, the LED board has been divided into quadrants, with each quadrant containing six thermocouples, three on the front and three on the back (see Table 5). Note that TCs 1–12 are located on the front of the board and TCs 13–24 are on the back side of the board. Plots of the thermocouple data for quadrant 4 are shown in Fig. 10. Further detailed plots will be presented during the discussions of the results.

Table 5 LED board quadrants and TC assignments

Quadrant	Assigned TCs
1	1–3, 13–15
2	4–6, 16–18
3	7–9, 19–21
4	10–12, 22–24

D. Data Anomalies

In reviewing the data from quadrants 1, 2, and 3, one of the first items to become apparent was the conspicuously low readings for TCs 3, 6, and 21. During the "all LEDs powered" periods, these three thermocouples provided readings up to 20°C below other thermocouples on that half of the board (see Fig. 11). The reason for this discrepancy is unknown. For TC 3 perhaps the strain relief for the power wires interfered with its temperature measurement, or perhaps for all three there was inadvertent contact in exposed thermocouple wires at a location other than the TC bead. Although not as pronounced, these TCs also provide low readings in the "inner LED ring powered" configuration as well. Interestingly, the TCs appear to provide accurate readings when there is no power flowing to the LEDs. Perhaps the exposed TC wires were in contact with the LED leads and this caused the TCs to register an incorrect temperature. Regardless of the reason, these three TCs are excluded from the data set.

A closer examination of TCs 7–9 in quadrant 3 also revealed an inconsistency. These three TCs are positioned such that TC 7 is closest to the inner ring of LEDs, TC 8 is embedded in the LED

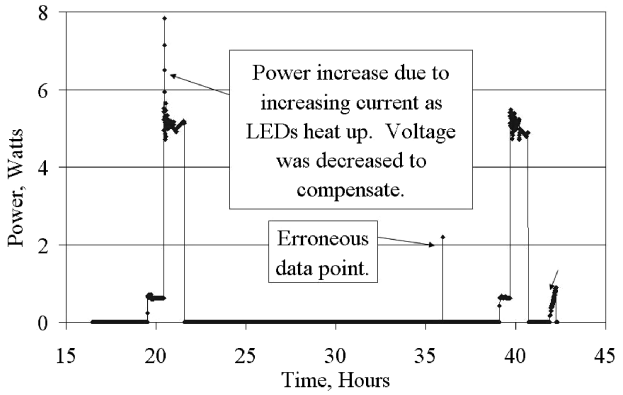

Fig. 8 Measured power profile during LED board test.

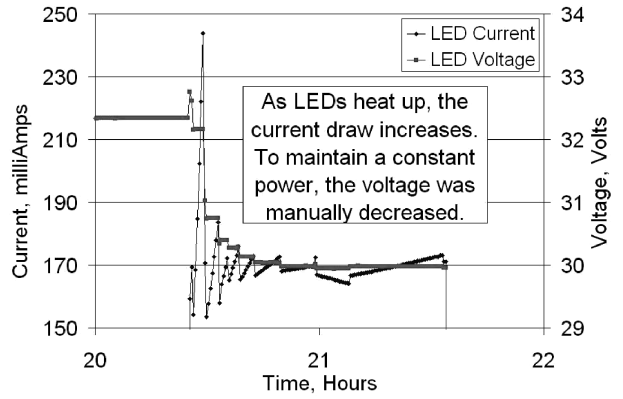

Fig. 9 Increasing LED current during first "all LEDs powered" configuration.

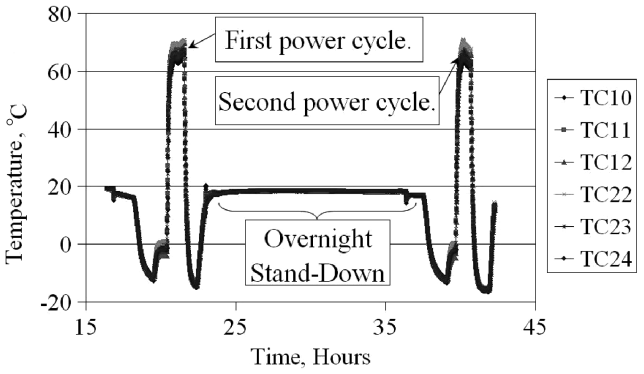

Fig. 10 LED board TC data as a function of time for quadrant 4.

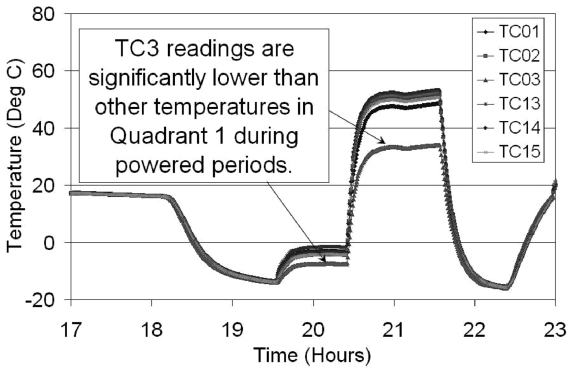

Fig. 11 Quadrant 1 data showing TC 03 lagging other temperature readings.

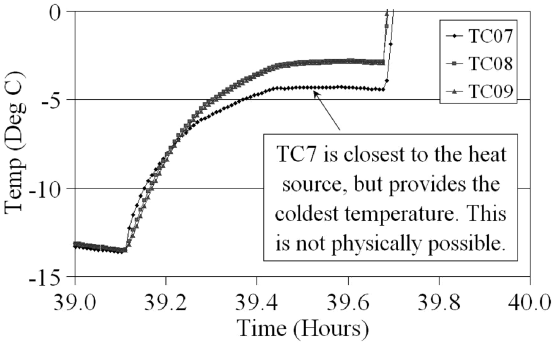

Fig. 12 Quadrant 3 data showing TC 7 registering cooler than TCs 8 and 9.

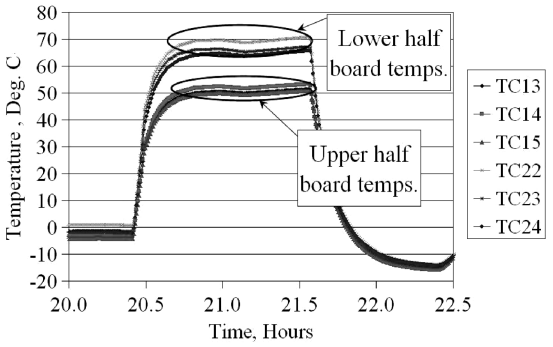

Fig. 13 Quadrant temperature difference between upper and lower halves of LED board.

cluster, and TC 9 is located on the outer edge of the board. Given this configuration, one expects TC 7 to have the highest temperature reading when the inner ring of LEDs was powered on and for the temperatures to decrease radially. Although this trend was seen in other quadrants, this was not the case for quadrant 3 TCs 7–9. During the first inner ring of LEDs powered cycle, these TCs showed minimal difference in temperature measurements. Figure 12 shows that during the second inner ring LED power cycle, TC 7 provides temperature readings less than TCs 8 and 9. This is not physically realistic. Because of the inconsistency with these readings, TCs 7–9 are excluded from the data set.

One final global trend to explore was the temperature difference between the upper and lower halves of the LED board. Temperatures for quadrants 1 and 2, on the upper half of the board, are up to 20°C cooler than temperatures for quadrants 3 and 4, on the lower half of the board when all LEDs are powered (see Fig. 13). The average temperature for quadrants 1 and 2 was close to 50°C, whereas for quadrants 3 and 4 it was approximately 66°C.

Because the LEDs are evenly distributed across the board, there should be a uniform heat flux on the board. However, there were 8 LEDs that were not functional in quadrant 2, which represents 10% of the LEDs on the upper half of the board. This difference in the heat flux between the upper and lower quadrants and the different radiation view factors because of the experimental setup could explain the difference in the temperatures. To investigate this possibility, a simple set of calculations was performed using the parameters presented in Table 6.

The total power into the board was 5.1 W. This power was then divided equally between all LEDs, and then the power on the upper and lower halves of the board could be calculated, accounting for the energy emitted by the LEDs as light (see Sec. IV.G below).

$$P_{\text{LED}} = \frac{P_{\text{total}}}{N_{\text{LED}}} = \frac{5.1\ \text{W}}{152} = 33.5\ \text{mW} \tag{11}$$

$$P_{\text{lower}} = (P_{\text{LED}} - 8)N_{\text{LED,lower}} - = 25.5 \times 80 = 2.04\ \text{W} \tag{12}$$

Table 6 Parameters for investigating nonfunctional LEDs effect on board temperatures

Parameter	Value
Time hack	21.35 h
I	170 mA
V	30 V
T_{sink}	−20°C
σ	5.67×10^{-8} W/(m^2·K^4)
ε	0.95
A_{surface}	4.335×10^{-3} m^2
N_{LED}	152 (80 on lower half, 72 on upper half)
LED radiant flux	8 mW/LED

$$P_{\text{upper}} = (P_{\text{LED}} - 8)N_{\text{LED,upper}} = 25.5 \times 72 = 1.836\ \text{W} \tag{13}$$

Once the heat dissipation for each half of the board was known, the average temperature for each half can be determined from the basic radiation heat transfer equation.

$$P = \varepsilon\sigma A_{\text{surface}}(T^4 - T_{\text{sink}}^4) \tag{14}$$

$$\begin{aligned} T_{\text{upper}} &= \left(T_{\text{sink}}^4 + \frac{P_{\text{upper}}}{\varepsilon\sigma A_{\text{surface}}}\right)^{1/4} \\ &= \left(253^4 + \frac{1.836}{0.95 \times 5.67 \times 10^{-8} \times 4.335 \times 10^{-3}}\right)^{1/4} \\ &= 57.7°\text{C} \end{aligned} \tag{15}$$

$$\begin{aligned} T_{\text{lower}} &= \left(T_{\text{sink}}^4 + \frac{P_{\text{lower}}}{\varepsilon\sigma A_{\text{surface}}}\right)^{1/4} \\ &= \left(253^4 + \frac{2.04}{0.95 \times 5.67 \times 10^{-8} \times 4.335 \times 10^{-3}}\right)^{1/4} \\ &= 63.6°\text{C} \end{aligned} \tag{16}$$

These results show that the nonfunctioning LEDs account for approximately 6°C of the overall 16°C temperature difference between the upper and lower halves of the board. An additional factor to consider is the lower half's view of the aluminum I-beam and the support plate. These surfaces are not actively cooled by the shroud and are therefore initially warmer than the −20°C shroud temperature. Because the lower half of the board has a larger view factor to these surfaces, it is reasonable to assume that these surfaces keep the lower half of the LED board warmer than the upper half.

Based on this assessment, the temperature difference between the upper and lower halves of the LED board can be explained by physical means. Therefore, no additional data needed to be discarded.

E. In-Plane Thermal Conductivity

The in-plane thermal conductivity was derived from the data recorded during the test periods when only the inner ring of LEDs was powered. Where possible the thermocouples along the inner and outer diameters were used because they produce the largest temperature gradient. However, in some instances the TC embedded in the LED array was used because of uncertainty in the accuracy of the TC along the outer or inner board diameter. Figure 14 shows how the data from the front of the board in quadrant 4 trends precisely as expected. TC 10 closest to the powered LEDs indicates the warmest temperature, whereas TC 12 on the outer diameter of the board registers the coldest temperatures.

Because the LED board is circular, the radial form of the conduction equation must be used. From this, the following expression for calculating the in-plane thermal conductivity can be derived:

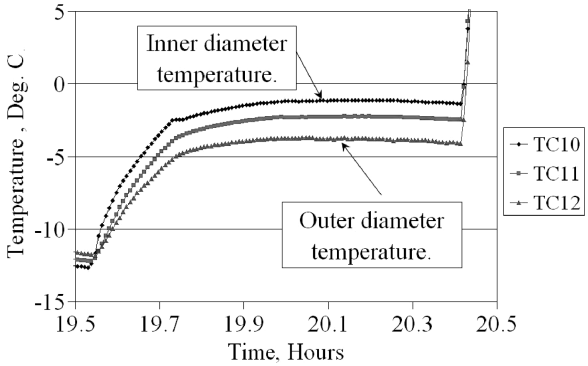

Fig. 14 Temperature difference between inner and outer board diameter when inner ring of LEDs is powered.

$$k = \frac{\dot{Q}\,\ell_n(r_2/r_1)}{2\pi t(T_1 - T_2)} \tag{17}$$

In addition to selecting the appropriate temperatures and radii, the correct heat load must also be selected. Because the board has been divided into four quadrants, it was assumed the amount of input power with the inner ring of LEDs on was equally divided between these four quadrants. Additionally, the LEDs' radiant flux must be accounted for. Therefore, the appropriate power for each quadrant was determined by taking the recorded input power, subtracting out the power emitted from the 20 LEDs that are on, and then dividing by four.

Tables 7 and 8 present the data used to calculate the in-plane thermal conductivity of the LED Board. Note that r_1 represents the inner diameter of the LED board, r_2 represents the approximate radius of the embedded thermocouples, and r_3 represents the outer radius of the board. These different radii were needed because of the exclusion of thermocouples as discussed earlier.

The measured in-plane thermal conductivity value of 4.9 W/(m · K) is only 13.5% of the pretest calculated value of 36.2 W/(m · K). This implies that the assumption that the copper layers are continuous does not hold true when compared with the test results. It is clear that for the LED board the low thermal conductivity of the dielectric material dominates. For other printed circuit boards that have a dedicated thermal plane, the conductivity may be slightly higher (especially along that plane), but for this particular board the FR-4 reigns.

F. Through-Plane Thermal Conductivity

The through-plane thermal conductivity was derived from the data recorded during the test periods when all LEDs were powered. Figure 15 illustrates the temperature difference across the thickness of the board that was used to determine the through-plane thermal conductivity.

For the through-plane thermal conductivity, the Cartesian form of the conduction equation can be used,

$$= kA_{cs}dT/dx \tag{18}$$

However, rather than attempt to determine the individual heat load at each thermocouple location, a heat flux was calculated based on the total heat input (minus energy emitted from LEDs) divided by the surface area of one face of the board,

$$\dot{Q}'' = \dot{Q}/A_{cs} = kdT/dx \tag{19}$$

In this equation, dx is the board thickness and dT is the delta T between thermocouples located on opposite sides of the board. To simplify the calculations, an average board temperature was computed for both the front and back of the board. The thermal conductivity can be found by rearranging the equation:

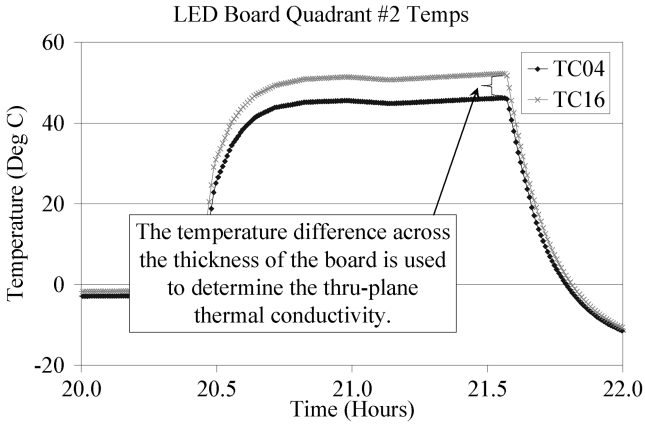

Fig. 15 ΔT across board thickness when all LEDs are powered.

$$k = \frac{\dot{Q}''t}{(T_2 - T_1)} \tag{20}$$

Table 9 presents the data for the measure through-plane thermal conductivity.

Two points immediately jump out when looking at these numbers. First, the back side of the board is, on average, warmer than the front side of the board, which is where the LEDs are located. Intuitively this does not make sense. It may be that the LED leads transport the heat to the back side of the board and that the emissivity associated with the LEDs is higher than the bare board. Another possible explanation is the location of the ground/signal layer within the board, which were not accounted for in this analysis. The second

Table 7 Temperatures used to calculate the in-plane thermal conductivity

Time hack = 20.2 h			Time hack = 39.6 h		
TC #	Temp	Radius	TC #	Temp.	Radius
TC 1	−3.0°C	r_1	TC 1	−4.0°C	r_1
TC 2	−4.3°C	r_2	TC 2	−4.9°C	r_2
TC 13	−1.5°C	r_1	TC 13	−2.1°C	r_1
TC 15	−4.2°C	r_3	TC 15	−4.7°C	r_3
TC 4	−2.8°C	r_1	TC 4	−3.7°C	r_1
TC 5	−5.8°C	r_2	TC 5	−6.9°C	r_2
TC 16	−1.6°C	r_1	TC 16	−2.3°C	r_1
TC 18	−4.1°C	r_3	TC 18	−4.6°C	r_3
TC 19	0.0°C	r_1	TC 19	−1.4°C	r_1
TC 20	−1.8°C	r_2	TC 20	−2.3°C	r_2
TC 10	−1.1°C	r_1	TC 10	−1.8°C	r_1
TC 12	−3.8°C	r_3	TC 12	−4.7°C	r_3
TC 22	0.0°C	r_1	TC 22	0.5°C	r_1
TC 24	−1.9°C	r_3	TC 24	−2.4°C	r_3

Table 8 Parameters used to calculate the in-plane thermal conductivity

Time hack = 20.2 h		Time hack = 39.6 h	
$\dot{Q}$	0.1165 W	$\dot{Q}$	0.11475 W
r_1	13.97 mm	r_1	13.97 mm
r_2	26.8 mm	r_2	26.8 mm
r_3	39.6875 mm	r_3	39.6875 mm
t	1.566 mm	t	1.566 mm
k_{1-2}	6.2 W/(m · K)	k_{1-2}	7.9 W/(m · K)
k_{13-15}	4.6 W/(m · K)	k_{13-15}	4.6 W/(m · K)
k_{4-5}	2.6 W/(m · K)	k_{4-5}	2.4 W/(m · K)
k_{16-18}	5.1 W/(m · K)	k_{16-18}	5.2 W/(m · K)
k_{19-20}	4.2 W/(m · K)	k_{19-20}	8.4 W/(m · K)
k_{10-12}	4.7 W/(m · K)	k_{10-12}	4.2 W/(m · K)
k_{22-24}	4.3 W/(m · K)	k_{22-24}	4.2 W/(m · K)
$k_{\text{in-plane}}$	4.9 W/(m · K)		

Table 9 Parameters used to calculate led board through-plane thermal conductivity

Time hack = 21.4 h		Time hack = 40.6 h	
$\dot{Q}''$	899.2 W/m^2	$\dot{Q}''$	822.3 W/m^2
t	1.566 mm	t	1.566 mm
$T_{\text{avg,front}}$	56.1°C	$T_{\text{avg,front}}$	52.6°C
$T_{\text{avg,back}}$	58.4°C	$T_{\text{avg,back}}$	55.6°C
k	0.60 W/(m · K)	k	0.42 W/(m · K)
$k_{\text{through-plane}}$	0.51 W/(m · K)		

point of interest is the fact that the measured through-plane thermal conductivity is higher than the calculated value. Once again this may be because of the large number of vias associated with LEDs and the fact that the LED leads and solder are efficiently transferring the heat to the back side of the board. The measured value of 0.51 W/(m · K) is approximately 53% higher than the calculated value of 0.32 W/(m · K).

G. Emissivity

To determine the LED board's emissivity, data from the portion of the test when all LEDs were powered was once again used. The average front and back surface temperatures were also used. At a steady-state condition, the emissivity of the board can be calculated from the basic radiation heat transfer equation

$$\dot{Q} = \varepsilon \sigma A_{\text{surface}} (T^4 - T_{\text{sink}}^4) \tag{21}$$

Table 10 shows the calculations of the board's emissivity using the data recorded during the test. Research revealed an approximate value for the radiant flux of each LED was 8 mW. When this amount of power times the number of LEDs was subtracted from input power, then the board's emissivity is measured as 1.00. Because an emissivity of 1.0 is unrealistic, a value of 0.95 will be used in the updated model. The fact that the measured emissivity was so high implies that the 8 mW radiant flux was not the correct value to use in these calculations. Unfortunately, no independent measurement of the LED's radiant flux was available at this time, and so the 8 mW was used in all calculations. Further investigation is needed.

H. Calculated vs Measured Thermophysical Properties

Table 11 shows a side-by-side comparison of the calculated and measured thermophysical properties. The difference between the two values was calculated as

$$\%\ \text{difference} = \frac{\text{calculated} - \text{measured}}{\text{measured}} \tag{22}$$

The fact that the calculated values for thermal conductivity were so different from the measured values highlights the importance of verifying model assumptions with test data.

V. Model Updates

With the measured thermophysical properties in hand, the thermal models were updated and an attempt to replicate the test data with model runs was made. In addition to updating the thermophysical properties, the aluminum I-beam structure and Teflon standoffs were also modeled. These components were included in an attempt to reproduce the temperature difference between the upper and lower halves of the LED board by accounting for alternate heat paths and radiation view factors. Further, the actual shroud temperature profile and power profile were used (refer to Fig. 8). Table 12 lists the changes made to the thermal model in an attempt to reproduce the test data.

Figure 16 plots the quadrant 1 model predictions and the test data for the first power cycle. Note that the initial model response was "fast." A possible reason for this was that the model does not include the shelf on which the test article rested during the test. The model does an adequate job of predicting the temperature values and spread

Table 10 Parameters used to calculate LED board emissivity assuming each LED emits 8 mW

Time hack = 21.4 h		Time hack = 40.6 h	
$\dot{Q}$	3.898 W	$\dot{Q}$	3.565 W
$T_{\text{avg,front}}$	56.1°C	$T_{\text{avg,front}}$	52.6°C
$T_{\text{avg,back}}$	58.4°C	$T_{\text{avg,back}}$	55.6°C
T_{sink}	−20°C	T_{sink}	−20°C
$\varepsilon_{\text{front}}$	1.04	$\varepsilon_{\text{front}}$	1.02
$\varepsilon_{\text{back}}$	0.99	$\varepsilon_{\text{back}}$	0.96
$\varepsilon_{\text{average}}$	1.00		

Table 11 Comparison of calculated and measured thermophysical properties

Property	Calculated value	Measured value	Difference
$k_{\text{in-plane}}$	36.2 W/(m · K)	4.9 W/(m · K)	638%
$k_{\text{through-plane}}$	0.32 W/(m · K)	0.51 W/(m · K)	−37%
ε	0.8	0.95	−15%

when the inner ring of LEDs was powered. When all LEDs were powered, the model overpredicts the response by approximately 10°C. Possible sources for this 10°C error in steady-state temperatures are errors in reading or computing input power, board emissivity, and LED radiant flux, as well as other factors such as errors in TC attachment and failure to account for fin losses from TC wires. However, the model captures the transient response of the board with considerable accuracy, as shown in the cooldown from the high temperatures.

Figure 17 demonstrates that the updated model does indeed predict a temperature difference between the upper and lower halves of the LED board. The model predictions indicate a spread of approximately 6°C between the halves, whereas measured data show almost 16°C between them. Interestingly, the model predictions were very close to the calculations performed in Sec. IV.D above. Those calculations predicted the upper half of the board to be close to 57°C and the lower half close to 63°C. Data trends for other quadrants were similar to those discussed in Fig. 16; no additional description is provided.

VI. Uncertainty in Measured Values

Although the test data provided the basis for an improved thermal model, several areas of uncertainty remain. The first cause of uncertainty was in the measurements themselves. These include the following:

1) Type-T thermocouple uncertainty, ±0.5°C.

2) Voltage uncertainty, quoted as 0.025% of scale (270 V)± 0.068 V.

3) Current uncertainty, quoted as 0.025% of scale (0.3 A) + 0.136% of reading (because of calibration curve inaccuracies).

4) Variations in shroud temperature, ±2°C.

The uncertainty in these measurements directly affects the calculated values for power, $k_{\text{in-plane}}$ [Eq. (17)], $k_{\text{through-plane}}$ [Eq. (20)], and ε [Eq. (21)]. To determine the magnitude of these

Table 12 Posttest thermal model updates

Pretest model parameter	Updated model parameter
Calculated thermal conductivity	Measured thermal conductivity
Assumed emissivity	Measured emissivity
Environment temp = −20°C	Measured shroud temperatures
Ideal power profile	Measured power profile
Power distributed across all LEDs	Power distribution takes into account eight nonfunctional LEDs
LED board floating in space	LED board connected to aluminum I-beam with Teflon standoffs

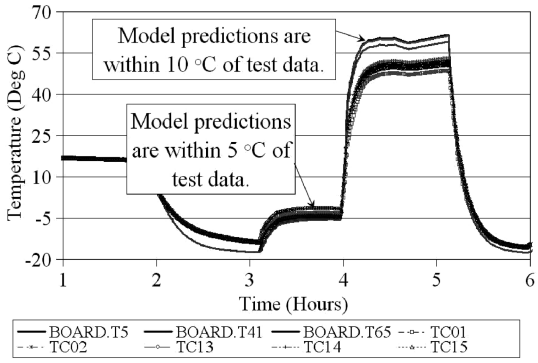

Fig. 16 Quadrant 1 model predictions and test data for first power cycle.

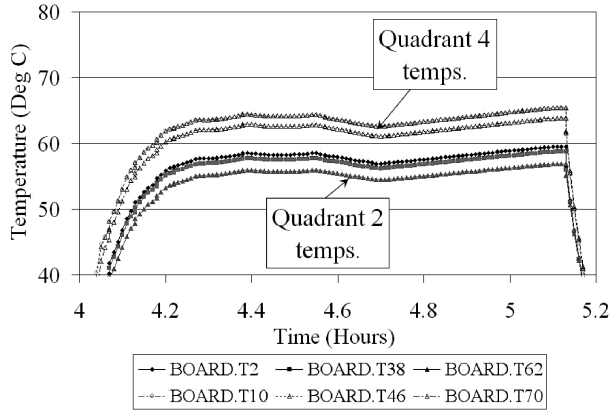

Fig. 17 Model prediction of temperature spread between upper and lower LED board halves.

effects, a Kline-McClintock error analysis was performed on each of the equations noted above. The results are presented in Table 13.

Additional sources of error are noted, but not included in the error analysis. These include the following:

1) LED board dimensions (from drawings rather than measured).

2) Thermocouples locations (estimated because of presence of LEDs).

3) Fin effects of the thermocouple wires.

4) Incorrect thermocouple installation.

5) The assumption that the radiant flux for each LED is 8 mW.

The authors feel compelled to emphasize the LED radiant flux as a particular gap in this paper. Without a reliable value for the LED's radiant flux, all calculations that depend on the measured power are potentially suspect. Obtaining a radiant flux measurement from the LEDs should be an integral part of any future testing.

One final uncertainty with the model was in regard to the test setup. The model assumes the LED board was attached to the aluminum I-beam. However, this assembly was "floating" in a spherical shroud in the thermal model. During the test, the assembly was resting on a test shelf that was not conditioned by the shroud. Additionally, the chamber door contained a window and was not conditioned. It is possible that these factors are contributing to some of the differences between the model predictions and test data.

Table 13 Summary of uncertainties

Equation	Typical value	Uncertainty
$k_{\text{in-plane}}$, Eq. (18)	4.9 W/(m · K)	±1.2 W/(m · K)
ε, Eq. (22)	0.95	±0.02

VII. Conclusions

The Mini-AERCam LED board was subjected to a thermal vacuum test to measure its thermophysical properties for use in a thermal model. After obtaining these values, the updated model was compared with test data and shows accuracy to within an uncertainty of ±10°C while capturing the board's transient response with considerable accuracy. The pretest calculations for the printed circuit board's in-plane thermal conductivity were grossly overestimated because of incorrect assumptions about the copper layers. The low-conductivity dielectric dominates the thermal network and leads to measured values of <5 W/(m · K). Similarly, the calculated value of the through-plane thermal conductivity was incorrect. Measured values were almost 150% greater than the predicted values. Future modeling of avionics board will take these results into account by preferentially weighting the thermal conductivities based on the dielectric component of the board.

References

[1] Fredrickson, S., Duran, S., and Mitchell, J., "Mini AERCam Inspection Robot for Human Space Missions," *Proceedings of AIAA Space 2004*, AIAA, Reston, VA, 2004.

[2] Fredrickson, S., Duran, S., Howard, N., and Wagenknecht, J., "Application of the Mini AERCam Free Flyer for Orbital Inspection," *Spacecraft Platforms and Infrastructure: Proceedings of the Society of Photo-Optical Instrumentation Engineers*, edited by Peter Tchoryk, Jr., and Melissa Wright, Vol. 5419, Society of Photo-Optical Instrumentation Engineers (International Society for Optical Engineering), Bellingham, WA, 2004, pp. 26–35.

[3] Fredrickson, S., Abbot, L., Duran, S., Jochim, D., Studak, W., Wagenknecht, J., and Williams, N., "Mini AERCam: Development of a Free Flying Nanosatellite Inspection Robot," *Proceedings of Society of Photo-Optical Instrumentation Engineer Aerosense 2003*, Society of Photo-Optical Instrumentation Engineers (International Society for Optical Engineering), Bellingham, WA, 2003.

[4] Williams, N., "Mini-AERCam Thermal Analysis Report," NASA Johnson Space Center Rept. 29894, Sept. 2002.

[5] Zaid, I., "Inspection Illuminator," NASA Johnson Space Center Drawing SDD39136571, April 2005.

[6] "Mini-AERCam LED Board Thermal Vac Test Procedure," NASA Johnson Space Center Task Performance Sheet TC0520006, July 2005.